I. Supplemental data items

Figure S1, related to Figure 2. Calculated C_T values for zDHHC RT-qPCR. Transcripts were considered below the limit of quantitation if the cycle threshold (C_T) values were above the amplification for control genomic DNA. PCR amplification efficiencies (E) were estimated by nonlinear regression of raw reaction progress curves and found to be similar (~0.9) among all PCR reactions (data not shown). Error bars represent standard deviations.

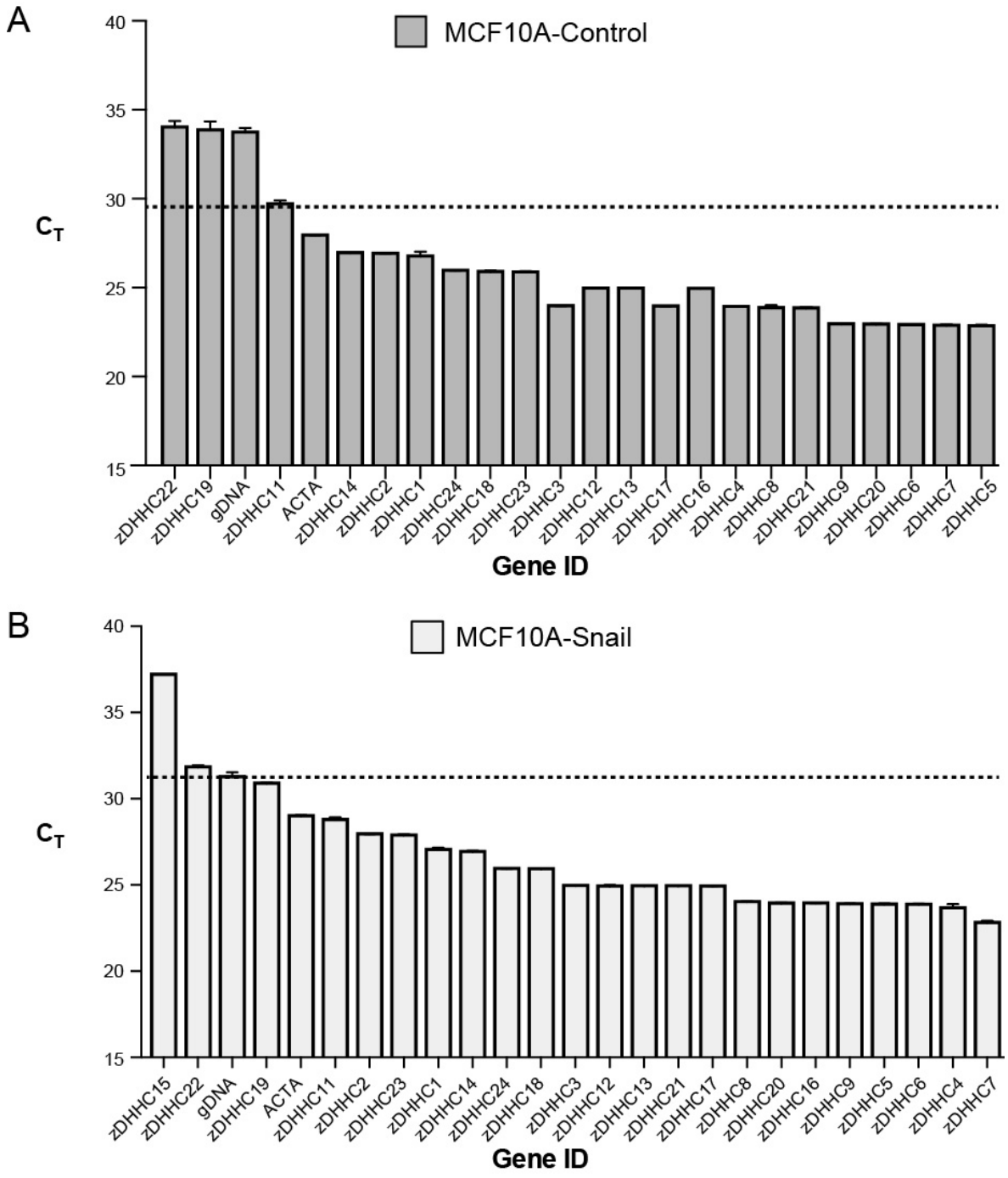

Figure S2, related to Figure 3. Scrib localization after inhibitor treatment in MDCK-Control cells and APT2 siRNA-mediated knockdown in MDCK-Snail cells. (A) Image processing workflow used to define masks to calculate perimeter localized Scrib by high content imaging (see **Supporting Experimental Procedures**). (B) Scrib localization is not affected by APT1 or APT2 inhibition in MDCK-Control cells. Images were analyzed as described in the Supporting Experimental Methods. (C) Western blot validation of APT2 knockdown in MDCK cells. EV = empty vector (Control), siControl = non-targeting siRNA control. Data is representative of 2 biological replicates run in triplicate. (D) Quantification of Scrib perimeter re-localization in MDCK-Snail cells by automated high-content microscopy. The percentage of perimeter-localized Scrib was calculated for each siRNA treatment according to the procedure outlined in the Supporting Experimental Methods. Asterisk indicates significant increase over control treatment in MDCK-Snail ($p < 0.001$). Error bars represent standard deviations.

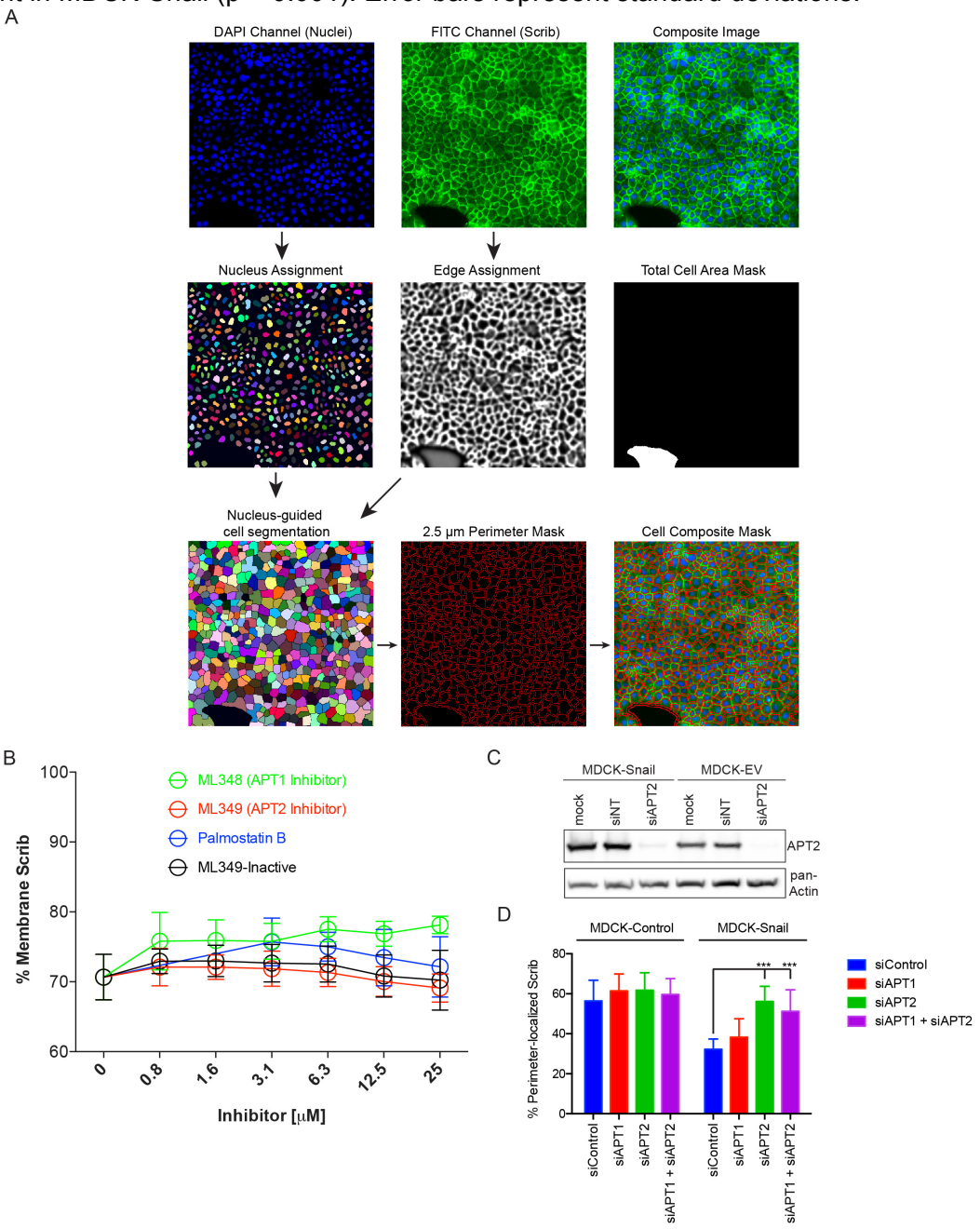

Figure S3, related to Figure 3. ML349 enhances perimeter localization of wild-type, but not the Δ22-Scrib N-terminal truncation mutant. (A) MDCK and MDCK-Snail cells were transiently transduced with retroviral vectors expressing either WT or Δ22-Scrib-GFP fusions, each tagged at the C-terminus to prevent interference with *S*-palmitoylation. Cells were treated overnight with 5 μM ML349 or DMSO vehicle, washed, and imaged for GFP fluorescence. Line intensity profiles across the junction of several dozen adjacent cells were quantified. The resulting curves fit to a Gaussian distribution (see **Supporting Experimental Methods**). (B) ML349-enhanced junctional localization requires the first 22 amino acids of Scrib. Quantified amplitude of cell-cell junction fluorescence intensity across ML349 treated MDCK cells. (asterisks: $p < 0.05$). Data is representative of independent biological replicates and analysis across dozens of individual cells. Error bars represent standard deviations.

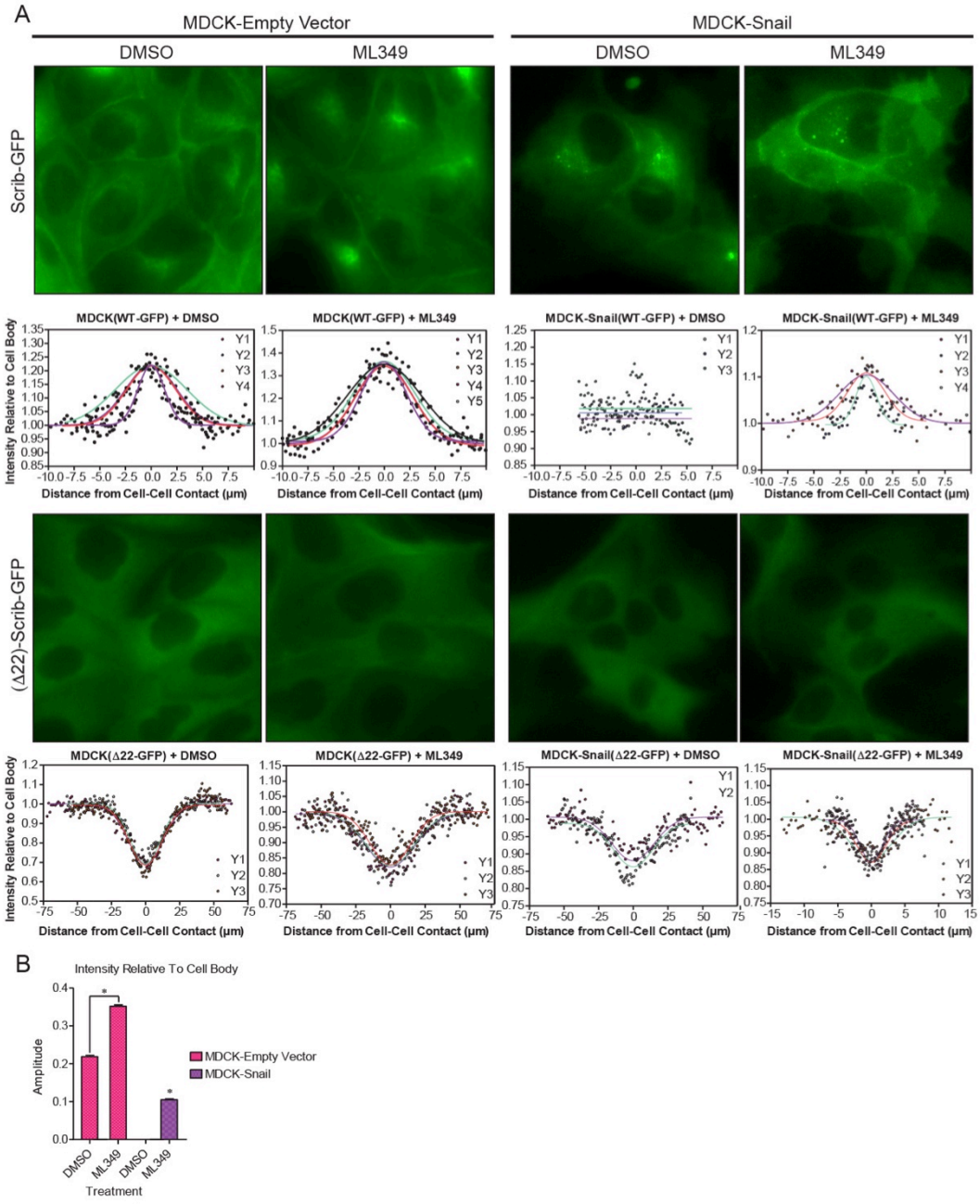

Figure S4, related to Figure 4. APT2 inhibition does not impair global 17-ODYA metabolic labeling. (A) ML349 pre-treatment does not alter the rate of 17-ODYA labeling in observable protein bands by in-gel fluorescence. MCF10A cells were incubated with either ML349 or DMSO vehicle control (0.1% v / v) for 3 hours, followed by addition of 17-ODYA for the indicated times (minutes). (B) The ~20 kDa protein band (presumably Ras) pulse-labels at the same rate in ML349-treated cells. 17-ODYA incorporation was quantified by dividing the signal intensity of the 20 kDa band in the Cy5 gel by the intensity of Coomassie bands from the corresponding lanes. (C) Neither ML348 nor ML349 overnight treatment alters the steady-state levels of incorporated 17-ODYA. Cells were incubated overnight with indicated inhibitor, followed by a 4 hour pulse with 17-ODYA. Lysates were conjugated to Cy5-N_3, separated by standard SDS-PAGE and visualized. Data is representative of two biological replicates analyzed in duplicate. Error bars represent standard deviations.

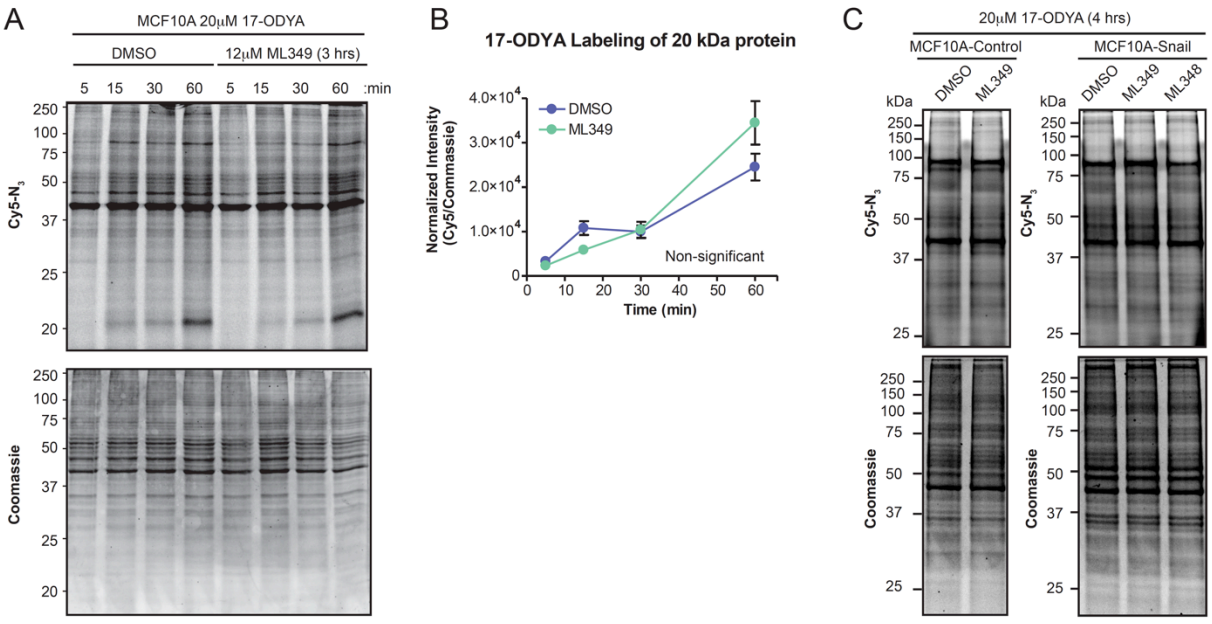

Figure S5, related to Figures 4 and 5. APT2 over-expression reduces Ras palmitoylation levels while isoform-selective APT inhibitors attenuate cell proliferation. (A) Acyl-biotin exchange assay performed on HEK293T cells over-expressing either pCDNA3 vector, APT2-GFP, or APT1-GFP. (B) Western blot validation of APT1 and APT2 overexpression. (C) Quantification of Ras palmitoylation levels demonstrates that APT2 over-expression, and to a lesser extent APT1, reduces Ras palmitoylation in non-polarized cells. (D) MCF10A and MCF10-Snail cells exhibit dose-dependent reduction in cell proliferation after overnight treatment with ML349. Multiple low magnification fields of view from a 96-well culture plate were imaged for DAPI fluorescence and counted using ImageJ software. Asterisks indicate statistically significant difference ($p < 0.05$) in cell viability between ML349 and the other treatments. Experiments were performed as biological duplicates and analyzed with duplicate technical replicates. Error bars represent standard deviations.

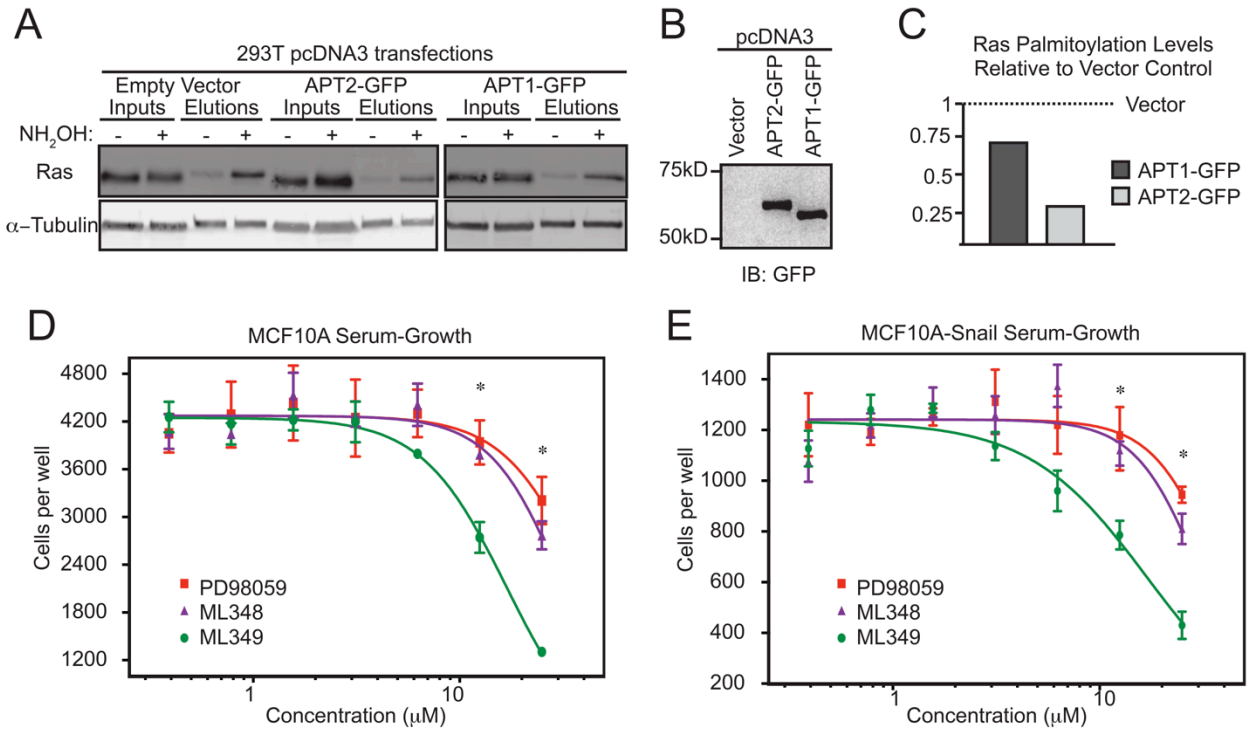

Table S1, related to Figure 2. SILAC analysis of FP-Biotin enrichments from MCF10A cells transduced with Snail or empty vector. Table S1 is included as a supporting Excel spreadsheet. SILAC ABPP serine hydrolase profiling with fluorophosphonate-biotin enrichment comparing MCF10A-Snail and MCF10A-Control cells, sorted by whether the enzyme is annotated as a serine hydrolase and the calculated SILAC ratio. Note that all annotated proteins are listed, including those not reported as serine hydrolases. Ratio is calculated as Snail / Control. Protein Entry = Uniprot protein identifier; Uniprot Accession = Uniprot protein accession; Protein Description = Uniprot Protein Name; SILAC Ratio = SILAC quantification ratio (Snail / Control Vector) of MS1 and MS2 ratios; Standard Deviation = Overall standard deviation; Quantified Events = Total number of MS1 and MS2 SILAC ratios computed per protein; p value: one-sample, two-tailed p-value against the expected ratio of 1.

II. Supplemental Experimental Procedures

Primary Antibodies

Species	Target Protein	Vendor	Catalogue Number	Dilution
Mouse	Scribble	Millipore	MAB1820	1:1000
Mouse	E-Cadherin	BD Bioscience	610181	1:5000
Mouse	α-Tubulin	Sigma	T6074	1:2000
Mouse	FLAG-M2	Sigma	F1804	1:5000
Rabbit	LYPLA1 (APT1)	Millipore	MABS166	1:500
Rabbit	LYPLA2 (APT2)	Pierce	PA5-27653	1:500
Rabbit	Phospho-Ser259 c-Raf	Cell Signaling	9421	1:500
Mouse	Ras	Millipore	50-171-675	1:1000
Mouse	MEK1/2	Cell Signaling	4694	1:500
Rabbit	Phospho-MEK1/2	Cell Signaling	9154	1:500
Mouse	Na+/K+ ATPase α-1	Millipore	05-369	1:2500
Rabbit	zDHHC2	Thermo Fisher	PA5-25504	1:500
Rabbit	zDHHC3	Abcam	ab124084	1:250
Rabbit	zDHHC5	Sigma	HPA014670	1:500
Rabbit	zDHHC7	Abcam	ab138210	1:500
Rabbit	zDHHC8	Sigma	HPA003422	1:1000
Rabbit	zDHHC20	Sigma	14273	1:500
Rabbit	zDHHC21	Abcam	ab103755	1:250
Mouse	zDHHC23	Sigma	SAB1409060	1:1000

Cell-cell junctional intensity analysis. MDCK and MDCK-Snail cells were transduced with puromycin-selectable retroviral pCLNCX vectors (Imgenex) expressing GFP-tagged Scrib fusion genes. Transduced cells were first selected with 10 μg / mL puromycin for two passage, and then plated on 6 cm dishes without selection. Cells at 80% confluency were treated in duplicate overnight with either 5 μM ML349 or DMSO vehicle for 16 hr, washed with PBS and imaged for GFP fluorescence with a Nikon Eclipse TE2000-S inverted epifluorescence microscope**.** Multiple fields were acquired per each plate for quantitation. Each acquisition collected both the bright field and GFP fluorescence. Images were imported into ImageJ software (NIH) where the bright field channel was thresholded to produce a binary mask to outline the cells. This mask was overlaid onto the corresponding fluorescent image, helping to correctly assign cell-cell junctions in the GFP channel. Next, perimeter localization was quantified by measuring line intensity profiles across the bright field-guided junctions of several dozen adjacent cells. Intensity values were imported into Graphpad Prism6. The raw values were converted to standard scores and were globally fit by nonlinear regression analysis to a Gaussian distribution calculating a shared fitted amplitude parameter.

High-content fluorescence microscopy. MDCK cells were plated at low density onto either 384-well or 96-well PerkinElmer ViewPlates using a 384 Reagent MultiDrop Dispenser (Thermo). Inhibitors were diluted in complete medium supplemented with dialyzed serum and added to sub-confluent cells using either the MultiDrop Dispenser or a multichannel pipettor (Rainin). Image acquisition was performed on an ImageXpress Micro XLS Widefield High-

Content Analysis System according to manufacturer's guidelines (Molecular Devices). Magnification settings were configured as 20X Plan Fluor without camera binning and gain values were empirically optimized for maximum signal-to-noise ratio. Plate acquisition methods were set to capture 4 corner sites plus a central site using predefined DAPI and FITC wavelength filter sets with a standard auto-focusing algorithm applied to the bottom of the plate per each acquired well. Each treatment was performed in 6 replicate wells, yielding 30 images for quantitative analysis representing more than 20,000 cells. Images were retrieved from the acquisition database and assembled into stacks for analysis using a custom Fiji macro in ImageJ (Schindelin et al., 2012), as outlined in the representative workflow image (see **Figure S2A**). More specifically, a local adaptive threshold was first applied to the DAPI channel to create individual cell seed points to assign nuclei. Another adaptive threshold was then applied to the FITC channel to separate foreground from background. The thresholded FITC image was then reconstructed relative to the defined nuclei to yield a total cell area mask. This mask was then used to exclude gaps in the cell monolayer where cell nuclei were absent. Next, an unsharp mask and Gaussian blur filter were applied to enhance the cell edges in the FITC channel, smoothing edges to remove any speckles from the image. This allowed for clear edge assignment in the populated cell area to define the perimeter of each cell. A marker-controlled grayscale watershed segmentation was performed on the processed FITC channel image, flooding from the nuclei-defined seed points to assign cell boundaries within the total binary mask area, forming the nucleus-guided cell segmentation map. This map was then used to create a cell boundary mask, which was widened to ~2.5 μm to create the cell perimeter mask, encompassing the membrane-localized fluorescence. This final mask was overlaid on the original, unprocessed FITC channel image to measure the total perimeter fluorescence, and inverted to calculate the total intracellular fluorescence. The data therefore represents the aggregate membrane fluorescence across the image, normalized by the total cell number. All masks were visually inspected to confirm accurate assignment of cell perimeter fluorescence before quantitation. Statistics were calculated across all 30 replicates for each condition. Higher concentrations of Palmostatin B demonstrated significantly higher standard deviation, likely due to increased cell blebbing and death, which increased the variance in the automated analysis.

Fiji Macro for Image analysis. This macro generates stacks of both total cell and membrane masks using the Fiji image analysis platform (Schindelin et al., 2012).

```
// Upload stacks for both DAPI and FITC channels in the same slice order.
// Adjust the brightness/contrast settings to display the full LUT range for each stack.
// Select the nuclear channel stack as the active window.

rename("RawDAPI");
run("Put Behind [tab]");
rename("RawFITC_a");
run("Duplicate...", "title=RawFITC_b duplicate");

// Prepare DAPI mask.
selectWindow("RawDAPI");
run("Enhance Contrast...", "saturated=0.4 normalize equalize process_all");
run("Subtract Background...", "rolling=50 stack");
run("8-bit");
run("Auto Local Threshold", "method=Mean radius=10 parameter_1=-10 parameter_2=0 white stack");
selectWindow("RawDAPI");
setOption("BlackBackground", true);
run("Fill Holes", "stack");
run("Despeckle", "stack");
run("Despeckle", "stack");
run("Despeckle", "stack");
```

```
run("Despeckle", "stack");
run("Despeckle", "stack");
run("Watershed", "stack");
run("Analyze Particles...", "size=50-Infinity circularity=0.50-1.00 summarize stack");
// The above string provides the nuclei count within each slice of the stack.

// Prepare FITC mask.
selectWindow("RawFITC_a");
run("Bandpass Filter...", "filter_large=1000 filter_small=1 suppress=None tolerance=5 autoscale saturate
process");
run("Subtract Background...", "rolling=50 stack");
run("Gaussian Blur...", "sigma=5 stack");
run("8-bit");

// For MDCK-Control, set parameter_1=1.5.
// For MDCK-Snail, set parameter_1=0.8.
run("Auto Local Threshold", "method=Phansalkar radius=1 parameter_1=0.8 parameter_2=5 white stack");

// Combine DAPI and FITC masks to generate total cell mask.
selectWindow("RawDAPI");
run("Duplicate...", "title=RawDAPI_b duplicate");
while (nSlices > 1) {
run("Make Substack...", "delete slices=1");
rename("RawDAPI_b_Slice");
selectWindow("RawFITC_a");
run("Make Substack...", "delete slices=1");
rename("RawFITC_a_Slice");
// For Mac users, replace the word "Geodesic" with "Morphological".
run("Geodesic Reconstruction", "marker=RawDAPI_b_Slice mask=RawFITC_a_Slice type=[By Dilation]
connectivity=8");
rename("TotalCellMask_Slice");
selectWindow("RawDAPI_b_Slice");
run("Close");
selectWindow("RawFITC_a_Slice");
run("Close");
selectWindow("RawDAPI_b");
}
// For Mac users, replace the word "Geodesic" with "Morphological".
run("Geodesic Reconstruction", "marker=RawDAPI_b mask=RawFITC_a type=[By Dilation] connectivity=8");
selectWindow("RawDAPI_b");
run("Close");
selectWindow("RawFITC_a");
run("Close");
run("Images to Stack", "name=TotalCellMask title=[] use");

// For MDCK-Control, proceed with fill holes function
// For MDCK-Snail, disable fill holes function (i.e. place the following before the argument below: //)
// run("Options...", "iterations=1 count=1 black pad do=Close stack");

// For MDCK-Control, set size=1000.
// For MDCK-Snail, set count=250.
run("Analyze Particles...", "size=250-Infinity show=Masks in_situ stack");
selectWindow("TotalCellMask");
run("Invert LUT");

// Prepare nuclear marker.
selectWindow("RawDAPI");
setOption("BlackBackground", false);
run("Dilate", "stack");
```

```
run("Invert", "stack");
selectWindow("RawDAPI");
while (nSlices > 1) {
run("Make Substack...", "delete slices=1");
rename("RawDAPI_Slice");
run("Analyze Particles...", "size=12.5-Infinity circularity=0.50-1.00 show=[Count Masks] clear in_situ");
selectWindow("RawDAPI");
}
run("Analyze Particles...", "size=12.5-Infinity circularity=0.50-1.00 show=[Count Masks] clear");
rename("RawDAPI_Slice");
selectWindow("RawDAPI");
run("Close");
run("Images to Stack", "name=NuclearMarker title=[] use");

// Initialize cell boundaries for mask generation procedure.
selectWindow("RawFITC_b");
run("Bandpass Filter...", "filter_large=40 filter_small=3 suppress=None tolerance=5 autoscale saturate
process");
run("Unsharp Mask...", "radius=10 mask=.7 stack");
run("Gaussian Blur...", "sigma=3 stack");

// Perform gray-level Watershed Segmentation on intialized FITC_b image.
while (nSlices > 1) {
run("Make Substack...", "delete slices=1");
rename("RawFITC_b_1");
run("Classic Watershed", "input=RawFITC_b_1 mask=None use min=0 max=65535");
selectWindow("RawFITC_b_1");
run("Close");
selectWindow("RawFITC_b");
}
run("Classic Watershed", "input=RawFITC_b mask=None use min=0 max=65535");
selectWindow("RawFITC_b");
run("Close");
run("Images to Stack", "name=Binary_watershed_lines title=[] use");
setMinAndMax(0, 1);
run("8-bit");
run("Auto Threshold", "method=Otsu white stack");
run("Invert LUT");
run("Invert", "stack");

// Perform Stack-enabled, marker-controlled watershed using nuclear marker,
// total cell mask and gray-level-watershed boundary input stacks.
selectWindow("TotalCellMask");
run("Duplicate...", "title=FinalTotalCellMask duplicate");
selectWindow("NuclearMarker");
while (nSlices > 1) {
run("Make Substack...", "delete slices=1");
rename("NuclearMarker_1");
selectWindow("TotalCellMask");
run("Make Substack...", "delete slices=1");
rename("CellMask_1");
selectWindow("Binary_watershed_lines");
run("Make Substack...", "delete slices=1");
rename("BinaryInput_1");
run("Marker-controlled Watershed", "input=BinaryInput_1 marker=NuclearMarker_1 mask=CellMask_1
calculate use");
selectWindow("NuclearMarker_1");
run("Close");
selectWindow("CellMask_1");
```

```
run("Close");
selectWindow("BinaryInput_1");
run("Close");
selectWindow("NuclearMarker");
}
run("Marker-controlled Watershed", "input=Binary_watershed_lines marker=NuclearMarker
mask=TotalCellMask calculate use");
selectWindow("NuclearMarker");
run("Close");
selectWindow("TotalCellMask");
run("Close");
selectWindow("Binary_watershed_lines");
run("Close");
run("Images to Stack", "name=CellBoundaryMask title=[] use");

// Perform final processing of cell boundary masks.
setMinAndMax(0, 1);
run("8-bit");
run("Auto Threshold", "method=Otsu white stack");
run("Invert", "stack");
setOption("BlackBackground", true);
run("Dilate", "stack");
run("Invert", "stack");
imageCalculator("Subtract create stack", "FinalTotalCellMask","CellBoundaryMask");
run("Invert LUT");
run("Skeletonize", "stack");
run("Convert to Mask", "method=Default background=Default");
rename("FinalCellBoundaryMask");
selectWindow("CellBoundaryMask");
run("Close");
setOption("BlackBackground", false);
```

III. Supporting Information References

Schindelin, J., Arganda-Carreras, I., Frise, E., Kaynig, V., Longair, M., Pietzsch, T., Preibisch, S., Rueden, C., Saalfeld, S., Schmid, B.*, et al.* (2012). Fiji: an open-source platform for biological-image analysis. Nat Methods *9*, 676-682.